

Q-STAC: Q-Guided Stein Variational Model Predictive Actor-Critic

Shizhe Cai¹, Zeya Yin¹, Jayadeep Jacob¹, and Fabio Ramos^{1,2}

¹University of Sydney ²NVIDIA

Abstract—Deep reinforcement learning (DRL) often struggles with complex robotic manipulation tasks due to low sample efficiency and biased value estimation. Model-based reinforcement learning (MBRL) improves efficiency by leveraging environment dynamics, with prior work [1]–[4] integrating Model Predictive Control (MPC) to enhance policy robustness through online trajectory optimization. However, existing MBRL approaches [5] still suffer from high model bias, task-specific cost function design, and significant computational overhead. To address these challenges, we propose Q-guided Stein Variational Model Predictive Actor-Critic (Q-STAC)—a unified framework that bridges Bayesian MPC and Soft Actor-Critic (SAC). Q-STAC employs Stein Variational Gradient Descent (SVGD) to iteratively optimize action sequences sampled from a learned prior distribution guided by Q-values, thereby eliminating manual cost-function engineering. By performing short-horizon model-predictive rollouts, Q-STAC reduces cumulative prediction errors, improves training stability and reduces computational complexity. Experiments on simulated particle navigation, diverse robotic manipulation tasks, and a real-world fruit-picking scenario demonstrate that Q-STAC consistently achieves superior sample efficiency, stability, and overall performance compared to both model-free and model-based baselines.

Index Terms—reinforcement learning, probabilistic inference, model predictive control, robotic manipulation, Stein variational inference.

I. INTRODUCTION

REINFORCEMENT Learning (RL) is widely used to solve complex control problems, ranging from autonomous vehicle navigation [6] to robotic control problems [7]. The superiority of RL lies in its ability to learn adaptive policies without requiring explicit dynamics modeling. By optimizing long-term cumulative return, RL is inherently suited for long-horizon decision-making problems. However, RL often suffers from poor sample efficiency, biased value estimation in long-horizon or sparse-reward settings, and unstable or unsafe behaviors during execution [8]–[10].

Model Predictive Control (MPC) [11], on the other hand, is a model-based receding horizon optimization algorithm. With accurate system dynamics modeling, MPC predicts future system states and iteratively optimizes a sequence of control inputs based on a predefined cost function, thereby gradually steering the system toward the desired target state. MPC produces interpretable and constraint-aware behaviors but typically relies on accurate models, task-specific cost

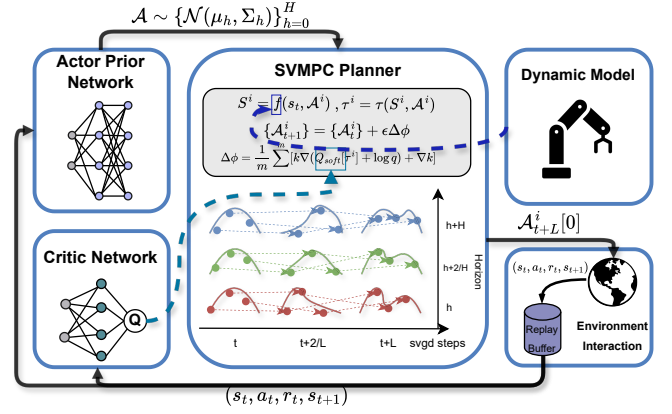


Fig. 1. Provides an overview of Q-STAC, which integrates a learned prior policy, short-horizon model predictive rollouts, and SVGD-based trajectory refinement under Q-value guidance. The framework unifies model-free policy learning and model-predictive optimization, enabling efficient action generation without hand-crafted cost functions.

design [12], [13]. Moreover, MPC optimizes control signals only within a limited prediction horizon at each step, which often leads to locally optimal solutions.

RL and MPC therefore offer complementary strengths—RL provides adaptivity and captures long-term rewards signal, whereas MPC provides safety, stability, and short-horizon optimality. Recent studies attempt to combine them [14], leveraging their complementary strengths to create a more stable and effective RL–MPC hybrid paradigm.

Following this motivation, we propose Q-guided Stein variational model predictive actor-critic (Q-STAC), a unified RL–MPC framework (Fig. 1). At each timestep, Q-STAC performs Bayesian inference over action sequences and applies Stein Variational Gradient Descent (SVGD) to approximate the policy posterior, using soft Q-values over short-horizon dynamics rollouts as the guiding signal. The first action in the optimized sequence is executed, while the same actions serve as improved learning signals for SAC-style actor and critic updates, yielding more stable and sample-efficient learning.

In contrast to prior RL–MPC hybrid approaches that either generate imagined rollouts for updates [15], [16] or learn dynamics models [1], [17], [18] and cost functions [2], [3], [19] to perform trajectory optimization with MPC, Q-STAC performs Bayesian MPC inference over the learned prior policy distribution, carrying out short-horizon optimization using SVGD. This avoids long-horizon model bias, reduces computational cost, and directly improves policy learning

This work has been submitted to the IEEE for possible publication. Copyright may be transferred without notice, after which this version may no longer be accessible.

stability.

We evaluate Q-STAC on 2D particle navigation, several robotic manipulation tasks, and a real-world fruit-picking scenario. The results show consistent improvements over both model-free and model-based baselines in robustness and overall performance. Ablation studies further validate the effectiveness of Q-guided optimization, and analyze the influence of horizon length, prior type, and the use of analytical versus learned dynamics. In summary, the Q-STAC framework brings several contributions to the field:

- We propose a unified RL-MPC framework that formulates action generation as a Bayesian model predictive control problem.
- We establish the theoretical connection between SAC and SVGD through the Soft Q-value, and extend this relationship to the trajectory level, enabling SVGD-based optimization within the RL-MPC framework.
- Extensive experiments on navigation, robotic manipulation tasks, and a real-world fruit-picking scenario demonstrate that Q-STAC achieves superior robustness, sample efficiency, and training stability compared to both model-free and model-based baselines.

II. RELATED WORK

A. RL-MPC Hybrid Methods

Recent research has increasingly focused on integrating RL with MPC to improve control stability, sample efficiency, and policy generalization. One line of work learns probabilistic ensemble dynamics models and leverages MPC for planning or policy improvement. For example, MBPO [15] and MOPO [16] generate short-horizon model rollouts for policy updates, while PETS [1] and PaETS [18] perform trajectory sampling and optimization using ensemble dynamics and variational inference. Similarly, TD-MPC [17] learns latent dynamics and value functions via temporal-difference learning and performs trajectory optimization. Another line of work assumes access to existing dynamics models and integrates them with RL via MPC-based planning. POLO [19] uses a learned value function as the MPC cost to plan actions online, while ACMPC [2] constructs a cost map from RL policies to guide differentiable MPC [20]. AC4MPC [3] further initializes MPC with actor-critic estimates as terminal costs. Unlike ACMPC and AC4MPC, which rely on hand-crafted cost functions or value-function terminal costs, Q-STAC provides a principled bridge between SVGD-based trajectory optimization and Q-value-guided policy gradients, offering a unified probabilistic view of trajectory-level policy improvement.

Previous work, such as MoPAC [4] shares similar ideas to ours. In particular, MoPAC performs trajectory optimization using MPPI based on manually designed cost functions and mixes model-predicted rollouts with real trajectories for training, whereas Q-STAC guides Bayesian MPC inference with Q-values.

B. SVGD-related Methods

Probabilistic inference helps control systems manage environmental and measurement uncertainties. SVGD [21] re-

formulates inference as an iterative update process and optimizes particles to approximate the target distribution. Various approaches have extended SVGD: SVMPC [12] and DuStMPC [13] apply it to Bayesian MPC for robust control. [22] proposes to combine probabilistic movement primitives with SVGD to handle multimodal trajectories for robot motion generation. Di-Plan [23] combines SVGD with diffusion models as informative priors and integrates path signatures to enhance diversity in the generated trajectories. Similarly, S²AC [24] utilizes SVGD to approximate the optimal policy distribution, but it focuses only on single-step policy optimization. In contrast, Q-STAC leverages model prediction to evaluate and optimize multi-step action sequences, thereby avoiding local optima and achieving more stable long-horizon performance.

III. PRELIMINARIES

Our approach builds upon the SAC framework [8] and Bayesian MPC [25], optimized via SVGD [21]. This section briefly outlines the SAC formulation and its policy-value update scheme, followed by an introduction to MPC, its Bayesian extension, and the fundamentals of SVGD.

A. Soft Actor-Critic

1) *Markov Decision Process*: We formulate the control problem as a policy search in an infinite-horizon Markov Decision Process (MDP) [26], defined by the tuple $(\mathcal{S}, \mathcal{A}, p, r, \gamma)$. Here, \mathcal{S} and \mathcal{A} denote the continuous observation and action spaces, respectively. The state transition function $p : \mathcal{S} \times \mathcal{A} \times \mathcal{S} \rightarrow [0, \infty)$ defines the probability density of the next state $s_{t+1} \in \mathcal{S}$ given the current state $s_t \in \mathcal{S}$ and action $a_t \in \mathcal{A}$. The reward function $r : \mathcal{S} \times \mathcal{A} \rightarrow [r_{\min}, r_{\max}]$ quantifies the quality of an action executed at a given state, and $\gamma \in [0, 1)$ is the discount factor that weights long-term rewards.

2) *Policy Learning and Q-value Update*: The objective of SAC is to learn a stochastic policy $\pi_\varphi(a|s)$ parameterized by φ , which maximizes both the expected cumulative discounted reward and the policy entropy:

$$J_\pi = \mathbb{E}_{(s_t, a_t) \sim \rho_\pi} \left[\sum_{t=0}^{\infty} \gamma^t (r(s_t, a_t) + \alpha \mathcal{H}(\pi(\cdot|s_t))) \right], \quad (1)$$

where α is the entropy temperature and ρ_π denotes the state-action marginal distribution under policy π . A higher entropy encourages more diverse actions, leading to better exploration and robustness.

SAC models the policy as an energy-based distribution, $\pi_\varphi(a|s) \propto \exp(\frac{1}{\alpha} Q(s, a))$, and optimizes it to jointly maximize the expected Q-value and policy entropy. This objective is formulated as follow to minimize the loss over replayed experiences \mathcal{D} :

$$J_\pi(\varphi) = \mathbb{E}_{s_t \sim \mathcal{D}, a_t \sim \pi_\varphi} [\alpha \log \pi_\varphi(a_t|s_t) - Q_\theta(s_t, a_t)], \quad (2)$$

The soft Q-function $Q_\theta(s_t, a_t)$, parameterized by θ , estimates the expected return and is optimized by minimizing the temporal-difference (TD) error:

$$J_Q(\theta) = \mathbb{E}_{(s_t, a_t) \sim \mathcal{D}} \left[\frac{1}{2} (Q_\theta(s_t, a_t) - \hat{Q}(s_t, a_t))^2 \right],$$

where $\hat{Q}(s_t, a_t) = r(s_t, a_t) + \gamma \mathbb{E}_{s_{t+1} \sim \mathcal{D}} [V_{\bar{\theta}}(s_{t+1})]$,

$$V_{\bar{\theta}}(s_{t+1}) = \mathbb{E}_{a_{t+1} \sim \pi} [Q_{\bar{\theta}}(s_{t+1}, a_{t+1}) + \alpha \mathcal{H}(\pi(\cdot | s_{t+1}))]. \quad (3)$$

Here, $\bar{\theta}$ denotes the parameters of the target Q-network, updated via exponential moving average.

B. Bayesian Model Predictive Control

MPC [11] optimizes a sequence of control signals $\mathcal{A}_t = (a_t, \dots, a_{t+H})$ over a finite horizon H using the dynamics model $s_{t+1} = f(s_t, a_t)$. The objective is to minimize a pre-defined cost function $C(c(\cdot, \cdot), c_{\text{term}}(\cdot))$, where $c(\cdot, \cdot)$ and $c_{\text{term}}(\cdot)$ denote step and terminal costs. MPC performs this optimization in a receding-horizon manner and executes only the first control a_t^* in the optimized sequence.

MPC can be reformulated as a Bayesian inference problem [12], [13], [25] by treating control inputs as random variables and inferring their posterior distribution conditioned on task outcomes or optimality criteria. Let $\tau = (S_t, \mathcal{A}_t)$ denote a state-control trajectory and $\mathcal{O}_\tau \in \{0, 1\}$ be a binary random variable indicating its optimality. We aim to infer the posterior distribution over optimal control sequences \mathcal{A} under the dynamics model f and the current state s_t using Bayes' rule (we omit $\mathcal{O}_\tau = 1$ as \mathcal{O}_τ for simplicity):

$$p_t(\mathcal{A} | \mathcal{O}_\tau; f, s_t) = \frac{p_t(\mathcal{O}_\tau | \mathcal{A}; f, s_t) p_t(\mathcal{A}; s_t)}{\int p_t(\mathcal{O}_\tau | \mathcal{A}; f, s_t) p_t(\mathcal{A}; s_t) d\mathcal{A}}. \quad (4)$$

Here, $p_t(\mathcal{A}; s_t)$ is the prior distribution induced by the current policy, and $p_t(\mathcal{O}_\tau | \mathcal{A}; f, s_t)$ is the likelihood that measures the probability of the trajectory being optimal under policy π_φ . This probabilistic view connects classical MPC with variational inference, providing a foundation for the Bayesian optimization mechanism used in Q-STAC.

C. Stein Variational Gradient Descent

SVGD [21] offers an efficient way to approximate complex posterior distributions with a set of particles $\{\mathcal{A}^i\}_{i=1}^m$. Given a step size ϵ , each particle is iteratively updated via:

$$\mathcal{A}^i \leftarrow \mathcal{A}^i + \epsilon \phi^*(\mathcal{A}^i), \quad (5)$$

where ϕ^* denotes the optimal perturbation direction in a reproducing kernel Hilbert space (RKHS) with kernel $k(\mathcal{A}', \mathcal{A})$, corresponding to the steepest descent direction of the KL divergence. The empirical estimate of ϕ^* is computed as:

$$\hat{\phi}^*(\mathcal{A}^i) = \frac{1}{m} \sum_{j=1}^m \left[\underbrace{k(\mathcal{A}^j, \mathcal{A}^i) \nabla_{\mathcal{A}^j} \log p(\mathcal{A}^j)}_{\text{Term ①}} + \underbrace{\nabla_{\mathcal{A}^j} k(\mathcal{A}^j, \mathcal{A}^i)}_{\text{Term ②}} \right], \quad (6)$$

where Term ① drives particles toward high-probability regions of p , and Term ② introduces repulsion to maintain particle diversity. SVGD thus provides a deterministic, non-parametric approach for approximate Bayesian inference, which we later employ in Q-STAC to optimize policy distributions.

IV. METHODOLOGY

In this section, we present our main contribution. Sec. IV-A outlines the overall architecture and describes the algorithmic flow of Q-STAC in detail. Sec. IV-B introduces the learned prior policy distribution, which provides initialization for short-horizon trajectory optimization. Sec. IV-C derives the Q-guided Stein variational inference procedure that connects SAC with Bayesian MPC. Sec. IV-D introduces the closed-form expression for computing policy entropy at the trajectory level. The complete algorithmic workflow is summarized in Alg. 1.

A. Overview

Q-STAC integrates SAC and Bayesian MPC within a unified framework. As illustrated in Fig. 1, the actor module in Q-STAC learns a Gaussian prior policy and samples initial action-trajectory particles conditioned on the current observation (detailed in Sec. IV-B). Then iteratively, it performs short-horizon model-predictive rollouts using the dynamics model to obtain future observation-action trajectories. The soft Q-values of these trajectories are evaluated by the critic, and SVGD iteratively refines the particles by treating the exponential of the soft Q-value as the optimality likelihood in the Bayesian MPC formulation (Sec. IV-C). Through this process, the action-trajectory particles progressively converge toward high-Q regions of the policy distribution.

During *inference*, we pick the action-trajectory particle that yields the **highest** trajectory Q-value, and execute its first action. During *training*, we **randomly** execute the first action from one of the particles to maintain exploration, and store the resulting transition in the replay buffer for network updates. The average action across particles is used when computing target values in Eq. (2) and Eq. (3).

B. Learned Policy Distribution as Prior

To enable faster convergence of action-trajectory particles, we initialize the policy distribution q_t^0 as a sequence of Gaussian distributions $\mathcal{N}(\mu_{t:t+H}, \Sigma_{t:t+H})$, where H denotes the trajectory horizon. The mean and covariance sequences $\mu_{t:t+H} \triangleq (\mu_t, \dots, \mu_{t+H})$ and $\Sigma_{t:t+H} \triangleq (\sigma_t, \dots, \sigma_{t+H})$ are obtained by conditioning a policy network on the current observation s_t : $(\mu_t, \Sigma_t) = \pi_\varphi(s_t)$, where φ denotes the network parameters. A set of M action-trajectory particles is then sampled from the Gaussian priors:

$$\{\mathcal{A}^i\}_{i=1}^M = \{a_{t:t+H}^i\}_{i=1}^M \sim \mathcal{N}(\mu_{t:t+H}, \Sigma_{t:t+H}), \quad (7)$$

where \mathcal{A} denotes an action-trajectory and the superscript i represents the i -th particle. As discussed in [24], we aim to learn an initial distribution close to the target posterior policy distribution so that the sampled particles can be efficiently shifted toward high-density regions after a few SVGD iterations.

To capture temporal correlations within the control horizon, we implement two alternative prior networks: a shared MLP with time-step embeddings, and a Recurrent Neural Network (RNN) for longer-horizon tasks. Although these architectural choices are not central to our contribution, they improve the expressiveness and stability of the learned prior distribution.

Algorithm 1 Q-guided Stein Variational Model Predictive Actor-Critic (Q-STAC)

Require: Initialize actor parameters φ , critic parameters θ , replay buffer \mathcal{D} , analytical dynamics model f , optional ensemble model f_ψ , kernel k , initial state s_0

```

1:  $s_t \leftarrow s_0$ 
2: for each timestep  $t$  do
3:   if using learned ensemble dynamics  $f_\psi$  then
4:     Update  $f_\psi$  on minibatch  $(s, a, s') \sim \mathcal{D}$ 
5:   end if
6:   Obtain policy prior:  $\mathcal{M}_t, \Sigma_t = \pi_\varphi(s_t)$ 
7:   Sample control particles:  $\mathcal{A} \sim \mathcal{N}(\mathcal{M}_t, \Sigma_t)$ 
8:   for each SVGD step do
9:     # Use  $f_\psi$  when using learned dynamics
10:    Rollout trajectories  $\tau = f(s_t, \mathcal{A})$ 
11:    Compute  $\hat{\phi}^*(\mathcal{A}^i)$  via Eq. (11)
12:    Update particles using Eq. (5)
13:   end for
14:   Select one optimized control sequence  $\mathcal{A}^i$ 
15:   Execute first action  $a_t \leftarrow \mathcal{A}^i[0]$  in environment
16:   Store transition  $(s_t, a_t, r_t, s_{t+1})$  in  $\mathcal{D}$ 
17:    $s_t \leftarrow s_{t+1}$ 
18:   for each policy update step do
19:     Sample minibatch from  $\mathcal{D}$ 
20:     Compute policy entropy via Eq. (12)
21:     Update critic  $\theta$  via Eq. (3)
22:     Update actor  $\varphi$  via Eq. (2)
23:   end for
24: end for

```

C. Stein Variational Inference Guided by Soft Q-values

The soft Q-value provides a natural bridge between SAC and Stein variational inference. In the following, we present a concise derivation that extends the single-step formulation in SAC to trajectory-level inference.

For a trajectory particle τ^i , its cumulative Q-value is defined as:

$$Q(\tau_t^i) = \sum_{h=0}^H Q(s_{t+h}^i, a_{t+h}^i). \quad (8)$$

Following the probabilistic inference view of reinforcement learning [25], the probability that a trajectory τ is optimal is modeled using a Boltzmann distribution over its expected return, assuming conditional independence of per-step optimality events:

$$p(\mathcal{O}_\tau | \tau_t) \propto \exp\left(\frac{1}{\alpha} Q(\tau_t)\right). \quad (9)$$

Substituting this likelihood into the Bayesian inference in Eq. (4), we obtain the posterior distribution for an individual trajectory particle:

$$\pi_\varphi^*(\tau_t^i | s_t) = p(\mathcal{A}_t^i | \mathcal{O}_\tau; f, s_t) \propto \exp\left(\frac{1}{\alpha} Q(\tau_t^i)\right) q^0(\mathcal{A}_t^i; s_t), \quad (10)$$

where $q^0(\mathcal{A}_t^i; s_t)$ denotes the Gaussian prior over the action-trajectory, as described in Sec. IV-B. Deriving the optimal maximum-entropy policy $\pi_\varphi^*(\tau_t^i | s_t)$ is therefore equivalent to

solving a trajectory optimization problem via approximate inference of this posterior distribution.

To approximate the posterior, we adopt Stein variational inference [12], [13], [21]. By substituting the log-posterior from Eq. (10) into the SVGD update, we can reformulate Eq. (6) as

$$\begin{aligned} \hat{\phi}^*(\mathcal{A}^i, s_t) = & \frac{1}{m} \sum_{j=1}^m \left[k(\mathcal{A}^j, \mathcal{A}^i) \nabla_{\mathcal{A}^j} \left(\frac{1}{\alpha} Q(\tau_t^i) + \log q^0(\mathcal{A}_t^i; s_t) \right) \right. \\ & \left. + \nabla_{\mathcal{A}^j} k(\mathcal{A}^j, \mathcal{A}^i) \right]. \end{aligned} \quad (11)$$

This formulation establishes a principled connection between Bayesian model predictive control and SAC, where the Q-value provides the gradient signal that guides the SVGD particle evolution toward high-value trajectories.

D. Entropy Computation

Q-STAC calculates policy entropy following S²AC [24], and further extends the formulation to the trajectory level. The resulting closed-form approximation is:

$$\mathcal{H}(\pi_\theta) \approx -\mathbb{E}_{\mathcal{A}^0 \sim q_0} \left[\frac{1}{H} \sum \left(\log q_0(\mathcal{A}^0) - \epsilon \sum_{l=0}^{L-1} \text{Tr}(\nabla_{\mathcal{A}^l} \hat{\phi}^*(\mathcal{A}^l)) \right) \right]. \quad (12)$$

Here, \mathcal{A}^l denotes the particle after l SVGD updates for L total SVGD steps. The trace term $\text{Tr}(\nabla_{\mathcal{A}^l} \hat{\phi}^*(\mathcal{A}^l))$ provides a first-order approximation of the log-density change induced by the SVGD variational mapping through the change-of-variables formula.

V. EXPERIMENTS

In this section, we first describe the experimental setup in Sec. V-A, including task definitions, the selection of baseline algorithms, and the dynamics model usage. We then present the main comparative evaluation in Sec. V-B, covering both training curves and success-rate analysis. Finally, in Sec. V-C, we investigate the effectiveness of Q-STAC through a series of ablation studies on Q-guidance, horizon length, prior design, and robustness under different dynamics models.

A. Experimental Setup

We evaluate Q-STAC on a set of continuous control tasks of increasing complexity, and validate its effectiveness across different domains compared with multiple model-free and model-based RL baselines. We first present the task setup:

1) *2D Particle Navigation Suite*: We design a set of 2D navigation tasks to jointly evaluate local obstacle avoidance and global path planning capabilities. In this environment, a point mass must reach a fixed target while avoiding Gaussian obstacles. The particle follows double-integrator dynamics, $\ddot{x} = u_x/m$ and $\ddot{y} = u_y/m$, where $u = (u_x, u_y)$ denotes control forces and m is the particle mass. State and control variables are bounded within ± 10 for position and acceleration, and ± 5 for velocity and control forces. The suite contains three difficulty levels: easy (Fig. 2(a)), medium (Fig. 2(b)), and hard (Fig. 2(c)) with increasing obstacle density and layout complexity.

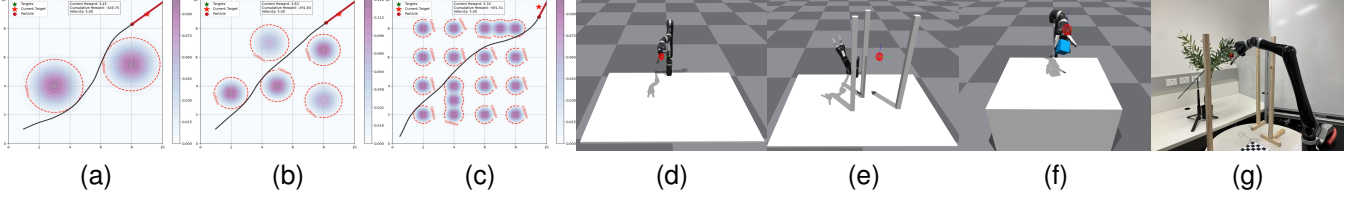


Fig. 2. Benchmark tasks used for algorithm evaluation: (a–c) 2D navigation tasks with multiple Gaussian obstacles, ranging in difficulty from easy to hard; (d–e) Kinova arm reaching tasks under two settings — without and with fixed obstacles; (f) Kinova pick-and-place task, demonstrating robotic manipulation involving picking and reaching motions; (g) Real-world Kinova arm setup.

2) *Kinova Manipulation Suite*: This suite consists of a series of robotic manipulation tasks implemented in the IsaacGym simulator [27] with the Kinova Gen2 Arm, which includes:

- **Reach**: A simple reaching task where the end-effector approaches a target region (Fig. 2(d)).
- **Reach (obstacle)**: An upgraded reaching task where the arm must navigate through constrained spaces and reach the target (Fig. 2(e)).
- **Pick and Place**: An object manipulation task requiring the arm to grasp a cube and hold it to a target area (Fig. 2(f)).

These tasks collectively evaluate the algorithms’ capabilities in robotic manipulation. The obstacle-based reaching task highlights improvements in stability and implicit safety achieved through MPC-guided control, while the pick-and-place scenario emphasizes Q-STAC’s effectiveness in long-horizon, contact-rich operations. The Kinova arm is controlled using joint-velocity commands, with six degrees of freedom for the arm and three for the gripper. To isolate policy learning from perception, target and object positions are provided in state space, avoiding the computational overhead of visual processing.

3) *Baseline Algorithms*: We compare Q-STAC with the following representative model-free and model-based RL baselines:

- **SAC** [8]: A maximum-entropy model-free actor-critic algorithm that serves as our main baseline for data efficiency and stability comparisons;
- **S²AC** [24]: An SVGD-based variant of SAC that performs particle-based policy optimization under the maximum-entropy framework, directly related to our variational formulation.
- **MBPO** [15]: A model-based policy optimization method that improves sample efficiency by using short-horizon model rollouts from a learned dynamics model.
- **PETS** [1]: A probabilistic ensemble-based model predictive control (MPC) algorithm that optimizes open-loop trajectories while accounting for model uncertainty.

For implementation, we adopt the open-source code from [24] for SAC and S²AC, and use the official `mbml-lib` implementations [28] for MBPO and PETS. Each method is trained with the same number of environment interactions and evaluated with five seeds to ensure fairness.

4) *Dynamics Model*: We experiment with both task-specific analytical dynamics models $f(s, a)$ and learned probabilis-

tic ensemble models $f_\psi(s, a)$ [1], [18] for the model-based baselines as well as for Q-STAC. For the 2D navigation tasks, we employ exact closed-form analytical dynamics. For the Kinova manipulation tasks, we construct an approximate analytical model using differentiable Kinova kinematics [29], where predicted observations are obtained via noisy kinematic propagation, following the physical laws of object contacts. Consequently, the analytical dynamics can still be substantially inaccurate compared with an oracle ground-truth dynamics model. The influence of these two model choices is evaluated through a model-type ablation study in Sec. V-C4.

In the comparative evaluation that follows, we adopt analytical dynamics for MBPO, PETS, and Q-STAC to isolate the effects of model-learning errors. However, following their original implementations, both MBPO and PETS additionally train a reward prediction model using an L2 regression loss.

B. Comparative Evaluation

1) *Overall Training Performance*: Fig. 3 illustrates the overall training performance across navigation and manipulation tasks. In environments with relatively simple dynamics (e.g., 2D Navigation), model-based methods such as MBPO and PETS converge rapidly in the early stages, reaching up to 80% of the maximum reward within the first 20k steps. However, their final performance saturates below the optimal reward, exhibiting instability and high sensitivity to reward-model inaccuracies. In contrast, model-free approaches can implicitly capture environmental dynamics and eventually learn more optimal policies with a larger number of environment interactions. Notably, Q-STAC and S²AC, both employing SVGD-based policy updates, achieve higher episodic rewards with fewer samples.

In complex Kinova manipulation tasks, where system dynamics are highly non-linear and contact-rich, MBPO and PETS struggle to maintain stable performance, particularly in the obstacle-avoidance and pick-and-place scenarios. Q-STAC consistently outperforms all baselines, converging faster and reaching higher normalized rewards across all tasks. It achieves up to 15% higher final rewards and reduced variance across runs, confirming its superior sample efficiency and stability.

2) *Success Rate Evaluation*: Task success rate provides a more direct and interpretable metric for robotic control than cumulative rewards. Tab. I summarizes the success rates of different algorithms on the Kinova manipulation tasks at 50%, 75%, and 100% of the total training progress, measured in

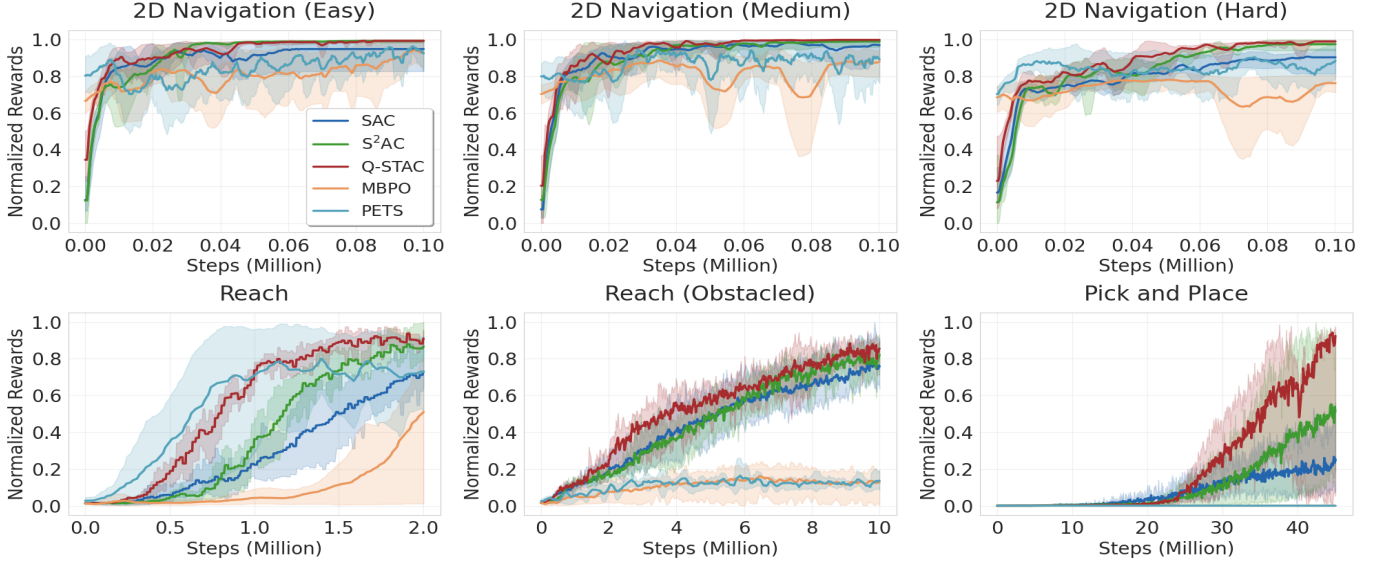


Fig. 3. Performance comparison of reinforcement learning algorithms across multiple control tasks. The figure displays training curves for five distinct algorithms (SAC, S^2 AC, MBPO, PETS, and Q-STAC) evaluated on the 2D navigation task suite and Kinova manipulation task suite. Each plot shows the normalized cumulative reward values (y-axis) against environmental steps (x-axis) measured in millions. Solid lines representing mean performance and shaded regions indicating standard deviation across 5 seeds.

TABLE I
SUCCESS RATE DURING TRAINING

Tasks	Algorithms	SR@50%	SR@75%	SR@100%
Reach	SAC	10.5 ± 3.00	17.0 ± 3.50	72.7 ± 3.00
	S^2 AC	1.40 ± 1.10	13.8 ± 3.80	79.4 ± 5.10
	MBPO	/	19.7 ± 3.70	56.3 ± 3.90
	PETS	49.3 ± 18.2	52.8 ± 7.70	72.2 ± 11.6
	Q-STAC	33.6 ± 3.70	55.0 ± 6.90	89.3 ± 1.90
Reach (Obstaced)	SAC	9.90 ± 2.60	37.4 ± 4.90	74.7 ± 3.50
	S^2 AC	10.2 ± 2.10	10.9 ± 1.90	78.9 ± 3.50
	MBPO	/	/	1.70 ± 1.50
	PETS	/	/	/
	Q-STAC	40.6 ± 3.00	45.4 ± 3.80	82.6 ± 4.40
Pick and Place	SAC	/	1.40 ± 1.20	80.9 ± 1.51
	S^2 AC	/	50.5 ± 7.00	82.7 ± 1.90
	MBPO	/	/	/
	PETS	/	/	/
	Q-STAC	1.20 ± 0.600	91.4 ± 1.70	95.3 ± 1.10

percentages (“/” indicates failure). For evaluation, checkpoints at these stages are tested across 10 episodes using 100 parallel environments per task. A trial is considered successful if the end-effector stays within 10 cm of the target for 20 steps in the reaching tasks, or within 5 cm after grasping the cube for 30 steps in the pick-and-place task. As shown in Tab. I, Q-STAC achieves the highest final success rates across all tasks while maintaining strong mid-training performance in both obstacle-reaching and pick-and-place scenarios. In contrast, model-based methods such as PETS show rapid early-stage improvement—achieving nearly 50% success rate in the simple reaching task—but fail to generalize to complex, contact-rich environments. Q-STAC outperforms the strongest baseline by up to 15 percentage points and exhibits lower variance across runs, confirming its robustness and sample efficiency.

3) *Performance Analysis*: Overall, Q-STAC exhibits superior sample efficiency, policy stability, and implicit safety compared with both model-free and model-based baselines. These advantages arise from replacing raw policy outputs with MPC-refined action sequences, which fundamentally reshapes the policy improvement process. Several key factors contribute to this performance gain. **(1) Higher-quality actor updates**: By optimizing action sequences over a short prediction horizon, Q-STAC leverages multi-step optimality signals rather than relying solely on single-step improvements. This reduces susceptibility to local optima and yields more coherent action sequences, leading to more stable and directed actor updates. **(2) More expressive policy representation**: The SVGD-based trajectory update enables approximate inference over multi-modal posterior distributions while maintaining particle diversity. As a result, the policy can represent richer behaviors than parametric policies used in SAC or S^2 AC. **(3) Stabilized critic learning**: MPC-optimized trajectories provide lower-variance value targets, facilitating faster convergence of the critic and improving overall training stability. **(4) Implicit safety via optimality inference**: Q-STAC does not require hand-designed safety constraints. Instead, unsafe or unstable trajectories naturally receive lower optimality likelihood through the soft Q-values, resulting in safer behavior without explicit constraint modeling.

C. Ablation Study

To further assess the Q-STAC’s design choices, we perform a series of ablation studies examining the influence of Q-guidance strength, learned prior policy, and the effects of different dynamics model types.

1) *Soft Q-Guidance*: We validate the effectiveness of the Q-value-guided SVGD optimization, by comparing the performance of SVMPC and Q-STAC on obstacle-avoidance tasks.

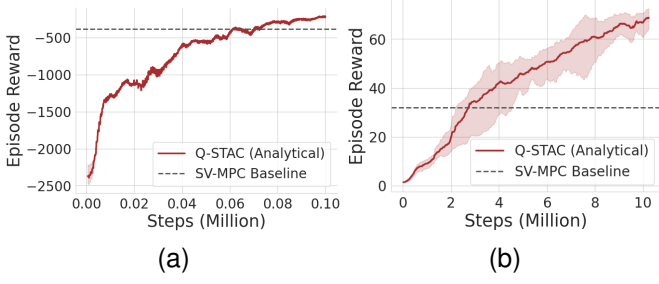


Fig. 4. Ablation results evaluating the effectiveness of Soft Q-Guidance on (a) 2D Navigation (Hard) and (b) Reach (Obstacle). The plot shows episodic rewards (y-axis) against environmental steps (x-axis) measured in millions.

SVMPC adopts the same dynamics model as Q-STAC, with its loss function and prior design following the implementation in [12]. As shown in Fig. 4, the black dashed line represents the episodic reward achieved by trajectories generated through SVMPC. We observe that Q-STAC outperforms SVMPC in both obstacle-avoidance tasks. While SVMPC performs reasonably well in the simpler 2D navigation task, Q-STAC demonstrates superior performance in the more complex manipulation-based obstacle-avoidance task, where the Q-value guidance captures long-term optimality that cost-based MPC cannot express, thus produces higher-quality trajectories.

2) *Different Prior*: Fig. 5(a) shows the training curves of Q-STAC in the Reach task under different prior distributions. The dashed lines correspond to two alternative priors: Random, which samples initial particles from a Gaussian distribution at every action step, and Mean, which samples from the mean action predicted by the current policy. For fairness, both variants use a fixed horizon of 3, and we increase their SVGD update steps and particle count to strengthen their optimization capability.

As illustrated in the figure, the Random prior fails to converge, while the Mean prior offers only early-stage improvement before collapsing as the action space grows more complex. These results demonstrate that the SAC-learned prior provides a much more informative initialization for Bayesian MPC, substantially reducing optimization complexity.

3) *Horizon Length*: The solid lines in Fig. 5(a) show the cumulative rewards achieved under different horizon lengths. As illustrated, with a short horizon (less than 3), the predicted trajectory window is too limited for the Q-values to provide effective guidance during optimization. Conversely, with a long horizon (greater than 7), accumulated model errors compound over time, leading to inaccurate Q-value estimates and reduced overall performance.

4) *Analytical and Learned Dynamics Model*: To examine how model errors affect different model-based algorithms, we compare the performance of MBPO, PETS, and Q-STAC when using a learned ensemble dynamics model versus analytical dynamics, across the 2D Navigation (Hard) and Reach tasks. As shown in Fig. 5(b), the benefit from accessing the analytical dynamics is negligible in 2D navigation task. However, in the manipulation task, analytical dynamics consistently yield higher performance than learned models. MBPO and PETS are particularly sensitive to model inaccuracies and exhibit

severe performance degradation in the Reach task. In contrast, Q-STAC shows only a minor drop in performance, indicating that it is substantially more robust to model bias. These results suggest that the effectiveness of Q-STAC does not rely on access to accurate analytical dynamics, but rather stems from its Q-guided SVGD optimization.

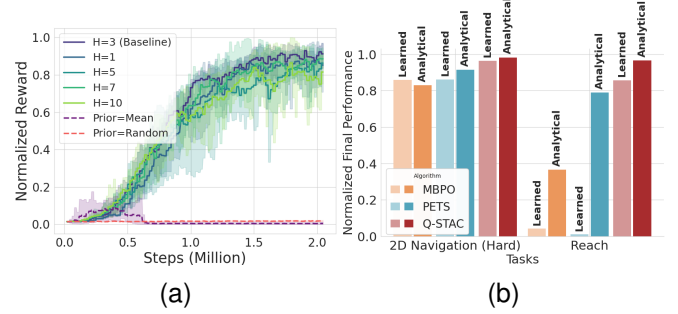


Fig. 5. Ablation results for (a) prior selection and horizon length for Reach Task with Q-STAC and (b) analytical vs. learned dynamics on 2D Navigation (Hard) and Reach (Obstacles) in model based RL.

D. Sim-to-Real

1) *General Setup*: We perform training and inference on a desktop machine equipped with an NVIDIA RTX 4090 GPU. A separate workstation runs the Kinova ROS API, which we interact with through a custom REST service over Ethernet. The Kinova arm is controlled via joint velocities, with a commanded control rate maintained at approximately 55–60 Hz.

2) *Adaptive Action Integration for Robot Control*: To mitigate the reality gap between simulation and real-world execution, we adopt a modified action integration strategy inspired by [30], [31]. The physical gap between reality and simulation, such as friction, damping, and stiffness often lead to accumulated steady-state errors during policy transfer. [31] proposes the Policy-Level Action Integrator (PLAI), which integrates actions over time via $s_{t+1}^d = s_t^d \oplus \pi(o_t)$ to improve robustness.

Following [30], we implement an adaptive action integrator. The RL policy outputs the desired joint velocity for the 6-DoF Kinova arm, $a_t = \pi(o_t)$. We compute segmented action updates as $\delta a_t^d = \frac{s_t - a_t}{n}$, where n is the segmentation factor used to feed the Kinova ROS controller at a higher frequency. The desired state is then updated via action integration:

$$s_{t+1}^d = s_t^d \oplus \delta a_t^d \quad (13)$$

$$s_t^d = \begin{cases} s_t & \text{if } i \% n = 0 \\ s_i^d & \text{otherwise} \end{cases}, \text{ for } i = 0, 1, 2, \dots, n$$

3) *Real Experiments*: We evaluate Q-STAC in a real-world scenario where a Kinova robotic arm must move across wooden obstacles and reach a designated position to pick a fruit hanging from a tree branch. This setup enables direct sim-to-real transfer from the Kinova-Reaching-with-Obstacles task. During the obstacle-traversal phase, control is executed fully online by the learned RL policy. After the arm reaches

TABLE II
REAL-WORLD TASK SUCCESS RATE

Task	Algorithms	Success Rate (%)	
		Avoiding Obstacles	Reaching Target
Real World Picking Fruit	SAC	20.0	40.0
	S ² AC	86.7	60.0
	Q-STAC	93.3	80.0

the target region, the gripper is manually closed to complete the picking motion. Fig. 2(g) illustrates the real-world setup, and Tab. II summarizes the success rates of SAC, S²AC, and Q-STAC, which are the only policies that successfully converged in the simulated Reach (Obstacled) task. Each policy is evaluated over 15 trials.

The results show that Q-STAC transfers reliably to the physical system, achieving the highest success rates in both obstacle avoidance and target reaching. SAC often behaves unstably and collides with obstacles, while S²AC avoids obstacles reasonably well but struggles to reach the target precisely. These findings demonstrate the advantage of Q-guided particle optimization, which yields more robust and geometry-aware actions under real-world perturbations such as unmodeled friction, joint backlash, and sensor latency.

VI. CONCLUSION AND FUTURE WORK

We introduced Q-STAC, a unified RL-MPC framework that formulates policy improvement as trajectory-level Bayesian inference guided by soft Q-values and optimized using SVGD. This formulation bridges SAC and MPC, enabling more directed exploration and robust policy updates through short-horizon model-predictive rollouts. Experiments across 2D navigation and Kinova manipulation tasks show that Q-STAC outperforms both model-free and model-based baselines. Ablation studies confirm the benefits of learned priors, Q-guided optimization, and robustness to model inaccuracies. In the future, we plan to incorporate visual observations into both reinforcement learning and dynamics modeling, enabling Q-STAC to tackle more complex and unstructured real-world robotic tasks.

REFERENCES

- [1] K. Chua, R. Calandra, R. McAllister, and S. Levine, "Deep reinforcement learning in a handful of trials using probabilistic dynamics models," *Advances in Neural Information Processing Systems (NeurIPS)*, vol. 31, 2018.
- [2] A. Romero, Y. Song, and D. Scaramuzza, "Actor-critic model predictive control," in *Proceedings of the IEEE International Conference on Robotics and Automation (ICRA)*. IEEE, 2024, pp. 14 777–14 784.
- [3] R. Reiter, A. Ghezzi, K. Baumgärtner, J. Hoffmann, R. D. McAllister, and M. Diehl, "Ac4mpc: Actor-critic reinforcement learning for nonlinear model predictive control," *arXiv preprint arXiv:2406.03995*, 2024.
- [4] A. S. Morgan, D. Nandha, G. Chalvatzaki, C. D'Eramo, A. M. Dollar, and J. Peters, "Model predictive actor-critic: Accelerating robot skill acquisition with deep reinforcement learning," in *Proceedings of the IEEE International Conference on Robotics and Automation (ICRA)*. IEEE, 2021, pp. 6672–6678.
- [5] T. M. Moerland, J. Broekens, A. Plaat, and C. M. Jonker, "Model-based reinforcement learning: A survey," *Foundations and Trends in Machine Learning*, vol. 16, no. 1, pp. 1–118, 2023.
- [6] B. R. Kiran, I. Sobh, V. Talpaert, P. Mannion, A. A. A. Sallab, S. Yogamani, and P. Pérez, "Deep reinforcement learning for autonomous driving: A survey," *IEEE Transactions on Intelligent Transportation Systems*, vol. 23, no. 6, pp. 4909–4926, 2022.
- [7] C. Tang, B. Abbatematteo, J. Hu, R. Chandra, R. Martín-Martín, and P. Stone, "Deep reinforcement learning for robotics: A survey of real-world successes," *Annual Review of Control, Robotics, and Autonomous Systems*, vol. 8, no. 1, pp. 153–188, 2025.
- [8] T. Haarnoja, A. Zhou, P. Abbeel, and S. Levine, "Soft actor-critic: Off-policy maximum entropy deep reinforcement learning with a stochastic actor," in *Proceedings of the International Conference on Machine Learning (ICML)*. PMLR, 2018, pp. 1861–1870.
- [9] S. Fujimoto, H. van Hoof, and D. Meger, "Addressing function approximation error in actor-critic methods," in *Proceedings of the 35th International Conference on Machine Learning (ICML)*. PMLR, 2018, pp. 1587–1596.
- [10] S. Gu, L. Yang, Y. Du, G. Chen, F. Walter, J. Wang, and A. Knoll, "A review of safe reinforcement learning: Methods, theories, and applications," *IEEE Transactions on Pattern Analysis and Machine Intelligence*, vol. 46, no. 12, pp. 11 216–11 235, 2024.
- [11] C. E. Garcia, D. M. Prett, and M. Morari, "Model predictive control: Theory and practice—a survey," *Automatica*, vol. 25, no. 3, pp. 335–348, 1989.
- [12] A. Lambert, A. Fishman, D. Fox, B. Boots, and F. Ramos, "Stein variational model predictive control," in *Proceedings of the Conference on Robot Learning (CoRL)*, 2020.
- [13] L. Barcelos, A. Lambert, R. Oliveira, P. Borges, B. Boots, and F. Ramos, "Dual online stein variational inference for control and dynamics," in *Proceedings of Robotics: Science and Systems (RSS)*, 2021.
- [14] R. Reiter, J. Hoffmann, D. Reinhardt, F. Messerer, K. Baumgärtner, S. Sawant, J. Boedecker, M. Diehl, and S. Gros, "Synthesis of model predictive control and reinforcement learning: Survey and classification," *arXiv preprint arXiv:2502.02133*, 2025.
- [15] M. Janner, J. Fu, M. Zhang, and S. Levine, "When to trust your model: Model-based policy optimization," *Advances in Neural Information Processing Systems (NeurIPS)*, vol. 32, 2019.
- [16] T. Yu, G. Thomas, L. Yu, S. Ermon, J. Y. Zou, S. Levine, C. Finn, and T. Ma, "Mopo: Model-based offline policy optimization," in *Advances in Neural Information Processing Systems (NeurIPS)*, vol. 33, 2020, pp. 14 129–14 142.
- [17] N. A. Hansen, H. Su, and X. Wang, "Temporal difference learning for model predictive control," in *Proceedings of the 39th International Conference on Machine Learning (ICML)*. PMLR, 2022, pp. 8387–8406.
- [18] M. Okada and T. Taniguchi, "Variational inference mpc for bayesian model-based reinforcement learning," in *Proceedings of the Conference on Robot Learning (CoRL)*. PMLR, 2020, pp. 258–272.
- [19] K. Lowrey, A. Rajeswaran, S. Kakade, E. Todorov, and I. Mordatch, "Plan online, learn offline: Efficient learning and exploration via model-based control," in *Proceedings of the International Conference on Learning Representations (ICLR)*, 2019.
- [20] B. Amos, I. Jimenez, J. Sacks, B. Boots, and J. Z. Kolter, "Differentiable MPC for End-to-end Planning and Control," in *Advances in Neural Information Processing Systems (NeurIPS)*, 2018.
- [21] Q. Liu and D. Wang, "Stein variational gradient descent: A general purpose bayesian inference algorithm," *Advances in Neural Information Processing Systems (NeurIPS)*, vol. 29, 2016.
- [22] Z. Yin, T. Lai, S. Khan, J. Jacob, Y. Li, and F. Ramos, "Stein movement primitives for adaptive multi-modal trajectory generation," in *Proceedings of the IEEE/RSSJ International Conference on Intelligent Robots and Systems (IROS)*. IEEE, 2024, pp. 11 901–11 908.
- [23] Z. Yin, T. Lai, L. Barcelos, J. Jacob, Y. Li, and F. Ramos, "Diverse motion planning with stein diffusion trajectory inference," in *Proceedings of the IEEE International Conference on Robotics and Automation (ICRA)*, 2025.
- [24] S. Messaoud, B. Mokeddem, Z. Xue, L. Pang, B. An, H. Chen, and S. Chawla, "S²ac: Energy-based reinforcement learning with stein soft actor-critic," in *Proceedings of the International Conference on Learning Representations (ICLR)*, 2024.
- [25] S. Levine, "Reinforcement learning and control as probabilistic inference: Tutorial and review," *arXiv preprint arXiv:1805.00909*, 2018.
- [26] M. L. Puterman, "Markov decision processes," *Handbooks in Operations Research and Management Science*, vol. 2, pp. 331–434, 1990.
- [27] V. Makovychuk, L. Wawrzyniak, Y. Guo, M. Lu, K. Storey, M. Macklin, D. Hoeller, N. Rudin, A. Allshire, A. Handa, and G. State, "Isaac gym: High performance gpu-based physics simulation for robot learning," *arXiv preprint arXiv:2108.10470*, 2021.

- [28] L. Pineda, B. Amos, A. Zhang, N. O. Lambert, and R. Calandra, “Mbrl-lib: A modular library for model-based reinforcement learning,” *arXiv preprint arXiv:2104.10159*, 2021.
- [29] G. Sutanto, A. Wang, Y. Lin, M. Mukadam, G. Sukhatme, A. Rai, and F. Meier, “Encoding physical constraints in differentiable newton-euler algorithm,” in *Proceedings of the 2nd Conference on Learning for Dynamics and Control (L4DC)*, vol. 120. PMLR, 2020, pp. 804–813.
- [30] J. Jacob, S. Cai, P. V. K. Borges, T. Bandyopadhyay, and F. Ramos, “Gentle manipulation of tree branches: A contact-aware policy learning approach,” in *Proceedings of the Conference on Robot Learning (CoRL)*. PMLR, 2024.
- [31] B. Tang, M. A. Lin, I. Akinola, A. Handa, G. S. Sukhatme, F. Ramos, D. Fox, and Y. Narang, “Industreal: Transferring contact-rich assembly tasks from simulation to reality,” in *Proceedings of Robotics: Science and Systems (RSS)*, 2023.